nature photonics

SUPPLEMENTARY INFORMATION

DOI: 10.1038/NPHOTON.2015.80

An integrated-nanophotonics polarization beamsplitter with 2.4 x 2.4μm^2 footprint

Bing Shen,[1] Peng Wang,[1] Randy Polson,[2] and Rajesh Menon[1]

[1]Department of Electrical and Computer Engineering, University of Utah, Salt Lake City, UT 84112, USA
[2]Utah Nanofabrication Facility, University of Utah, Salt Lake City, UT 84112, USA

In the supplementary information, design algorithm (section 1), insight into the numerical design (section 2), tolerance to fabrication errors (section 3), experiment (section 4), movie description (section 5) and fabrication steps (section 6) are given in detail.

1. Design

The direct-binary-search (DBS) algorithm was successfully adapted to design broadband diffractive optics for spectrum manipulation [1] and to design nanophotonic devices [2,3]. Here again, the DBS algorithm is extended to design the metamaterial polarization beam splitter. Inverse design algorithm, which ends up with designs with performance parameters first specified, was implemented in nanophotonic design previously [4]. However, the designs achieved with inverse design algorithm typically exhibit a continuous topography, which leaves them to be complicated for fabrication [4]. DBS algorithm, however, first discretizes an area into a number of digital pixels and then works to achieve a particular combination of all the pixels, whose electromagnetic performance is closest to the specification first given. The dimension of the individual pixel is determined by the fabrication capacity. For our case, Focused ion beam (FIB) is employed in the fabrication and as a result, the pixel dimension is 120nm by 120nm that is readily achieved by FIB. In the following part, we would discuss the two essential parts of the design algorithm: DBS optimization algorithm and FDTD calculation.

1.1 Direct-binary-search (DBS)

As is known to all, there are a number of optimization algorithms available for designing complex nanophotonics structures, including Newton's iteration, simulated annealing, genetic algorithm and etc. As a matter of fact, we have tried both simulated annealing and DBS algorithm and found that DBS ends up with a comparable design with simulated annealing but at a much higher speed. This is due to the fact that simulated annealing is capable of encompassing global maximum while DBS only tries to encompass the local maximum [5]. Simulated annealing is advantageous when only there are only a few corners with FOMs that are close in value to the absolute global maximum. However, if there are many corners in the hypercube with FOMs that are close to the absolute global maximum, the difference in terms of optimization results between DBS and simulated annealing is not significant. That is to say, the sacrifice of computation time in simulated annealing would not necessarily give us better results. For our case, we believe that there are a number of possible pixel combinations that could exhibit comparable performances with the global maximum. As a result, DBS would end up with a comparable design simulated annealing but consumes far less time. However, since DBS is sensitive to starting point and tend to suffer from premature convergence in local optima [1,2]. As a result, we repeated the process with several random starting designs generated by Matlab. Due to the fact that different initial cases would end up with different optimal designs, the optimized design presented in the manuscript is the best design with the largest FOM. The following is the essential steps of DBS.

First: initialization. For our particular case of polarization beam splitter, we discretize an area of 2.4 mm × 2.4mm into 20 × 20 pixels, each of sizing 120 nm × 120nm. The possible pixel states are silicon and air where silicon is etched away. In DBS, the two states are denoted by 1

DOI: 10.1038/NPHOTON.2015.80

and 0. It should be noted that our algorithm is also open to quaternary, octonary, and hexadecimal states. For example, in octonary states system, 000 means that silicon is totally etched away and 001 means that an eighth of silicon is etched away which means that the height of the silicon pillar is 15 eighths of the original one. This allows for a new freedom in design although a gray scale lithography is needed in fabrication. Another type of parameter besides the pixel states to be optimized is the device thickness. An upper bound of 500nm is imposed on the device thickness for ease of fabrication. The device thickness is then digitalized with a predefined perturbation, 10nm for our case. A totally random starting point is used in our optimization. The figure-of-merit (FOM) for optimization is defined as the averaged transmission efficiency for TE and TM. However, a large extinction ratio could also be achieved, where FOM is replaced by weighted average of transmission efficiency and extinction ratio in each arm.

Second: order sequence generation. Matlab is used to generate a totally random sequence. The order of the pixels and device thickness to be perturbed is determined by the sequence.

Third: perturbation. For the perturbation of pixel state, we first toggle the pixel state and evaluate the FOM. If FOM is improved, then new pixel state is kept and the next pixel is toggled. Otherwise, the original pixel state is kept. While for the perturbation of device thickness, we first apply a positive perturbation to it and evaluate FOM. If FOM is improved and the search moves to the next parameter (pixel state). Or, we apply a negative perturbation (same absolute value but of opposite sign) to device thickness and re-evaluate the FOM. If it is improved, the negative perturbation is kept and moves to the next parameter. If FOM is not improved in both positive and negative perturbation, the original device thickness value is kept.

Fourth: termination. One iteration ends when all the 20 × 20 pixel states and the device thickness are addressed. The whole optimization process ends when the total iterations reach maximum (402 for our case), or the FOM exhibits no improvement after one iteration, or the improvement is smaller than a threshold (< 0.5% for our case).

1.2 FDTD

Finite-difference time-domain (FDTD) is employed for FOM evaluation. Some key factors that matter a lot to our design are summarized as follows.

Refractive index of silicon. Since our design is aimed for optical telecommunication (~1550nm), the refractive index of silicon at 1550nm is needed. Although measured refractive index for silicon at 1550nm is readily available in many literatures, we manually calculate the refractive index by ourselves. Since the feature size of our structure is in deep subwavelength, some factors including the fabrication technology of Silicon-on-insulator (SOI) wafer, grain size, and etc. may have an impact on the refractive index of silicon. As a result, it is beneficial to retrieve the refractive index of silicon for the particular SOI used for fabrication before carrying on optimization. For our case, we, however, take a clumsy way that should be improved in our future research. We fabricate an on-chip polarizer (as shown in Fig. S4) and evaluate its performance with FDTD method. The refractive index of silicon is taken from 3.2 to 4.0, and we pick the refractive index whose corresponding performance is closest to the measured performance.

Simulation resolution in FDTD. Setting an appropriate resolution is essential since this would decrease calculation time consumption without sacrificing precision. We have tried different resolutions and found that grid size of 30nm meet our needs. The simulated field pattern exhibits negligible change as with the increase of resolution. The simulated field patterns with 30nm-grid and 20nm-grid are summarized in Fig. S1. The negligible difference between the two reveals that 30nm-grid size meet our needs.

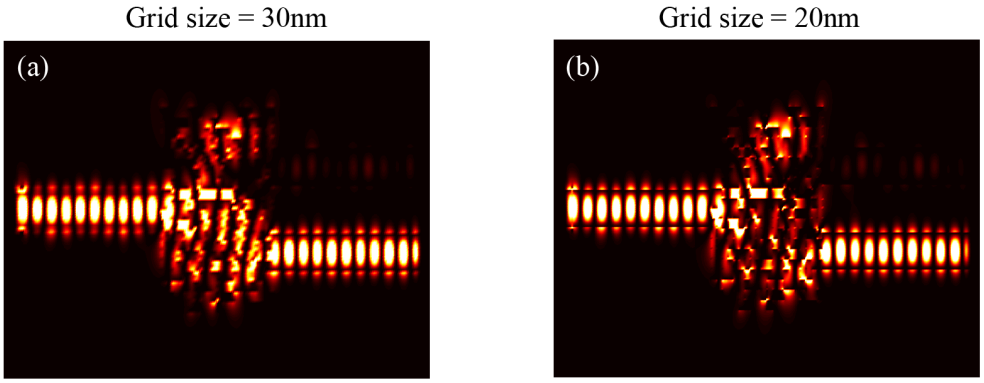

Fig. S1. Simulated TE field patterns for PBS with different simulation resolution. (a) 30nm grid size and (b) 20nm grid size. The averaged difference between the two is less than 1%.

2. Insights into numerical design

To further elucidate the operation of the metamaterials PBS, we re-ran the optimization with a pre-designed starting point instead of a random one that is typically employed. The pre-designed structure is shown in the inset of Fig. S7 (the bottom structure). The input and output (top) waveguide for TM polarization is directly connected by a discretized inclined silicon waveguide, while the rest of the splitter is filled with random-distributed silicon pixels to best match the guiding mechanism discussed above. In this case, the two final optimized devices exhibit similar performance. However, the design with a pre-designed starting point converges much faster, which suggests that the guiding mechanism implied earlier is reasonable.

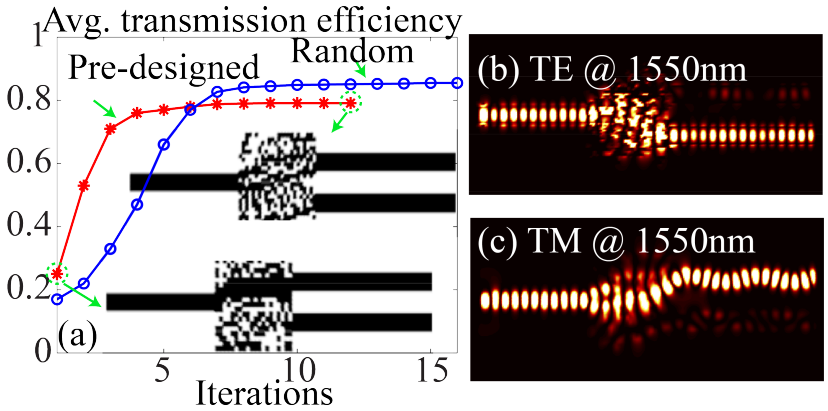

Fig. S7: Optimized design with pre-designed starting point. (a) Evolution of the averaged transmission efficiency as a function of the iteration number for both the optimization designs with random (blue curve with circle) and pre-designed (red curve with star) starting point. The optimized (top) and pre-designed starting (bottom) design is shown in the inset. Field pattern of (b) TE and (c) TM polarized light for optimized structure with a pre-designed starting point.

3. Tolerance to fabrication errors

In general, there are several types of fabrication errors involved in our particular fabrication method. In the manuscript, we have investigated our device's robustness to device thickness, which is the most likely fabrication error for our device. However, in our fabrication process, we have also found that position shift is likely to occur as well. This is due to the fact we adopted a two-step fabrication process and precise alignment between the 3mm-wide waveguide (made in the first step) and metamaterials (made in the second step) is actually needed. In addition, fabrication error in the size of each of the pixels in the 2.4 um × 2.4 um area is worth investigation as well. In this part, we theoretically analyze our device's tolerance to both the two types of fabrication errors.

DOI: 10.1038/NPHOTON.2015.80

3.1 Alignment error in mode-converting PBS

A fraction of the nanophotonic PBS is missing if there is an alignment error between the 3μm-wide waveguide and the nanophotonic PBS, which deteriorates the performance. The mode-converting PBS's performance as a function of position shift is theoretically analyzed and the results are summarized in Fig. S8. The results reveal that our device is pretty robust to fabrication errors.

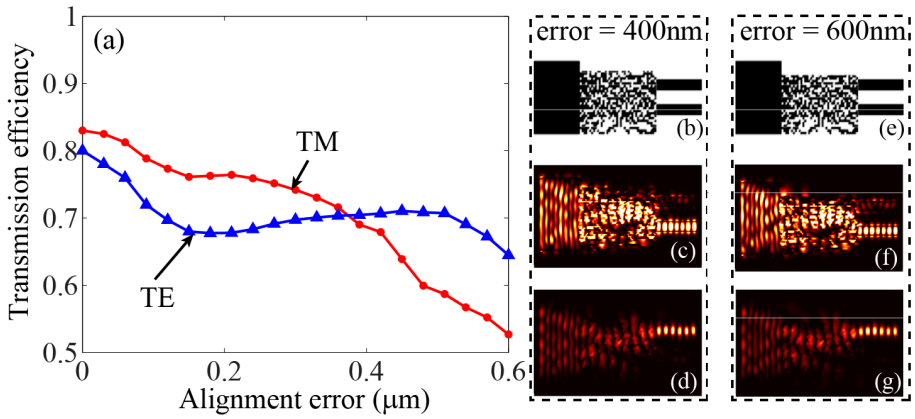

Fig. S8. Sensitivity to alignment error. (a) Transmission efficiency as a function of alignment error. (b) Epsilon distribution, (c) TE field pattern and (d) TM field pattern for alignment error of 400nm. (e) Epsilon distribution, (f) TE field pattern and (g) TM field pattern for alignment error of 600nm.

3.2 Dimension error in PBS

We scale the dimension of the PBS and then theoretically get the performance as a function of dimension errors with regard to the design dimension. The results are shown in Fig. S9. The dimension scaling error has little impact on TM mode but not on TE mode. This is expected since light in TM mode is mainly confined in the Z direction and thus is insensitive to the scaling errors in plane, which does not hold true for TE in which case light is mainly confined in XY direction. Anyway, scaling error over 100nm brings a 3dB drop to the transmission efficiency of TE mode.

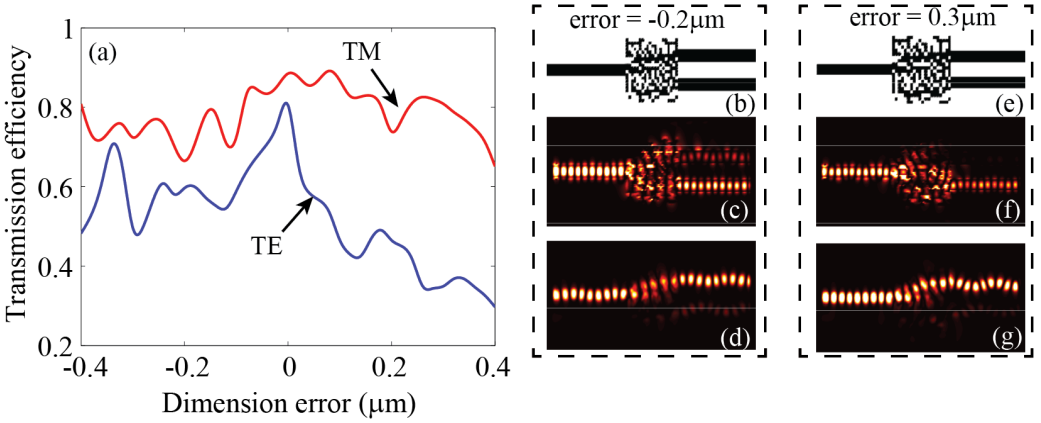

Fig. S9. Sensitivity to alignment error. (a) Transmission efficiency as a function of alignment error. (b) Epsilon distribution, (c) TE field pattern and (d) TM field pattern for alignment error of 400nm. (e) Epsilon distribution, (f) TE field pattern and (g) TM field pattern for alignment error of 600nm.

4. Experiment

In this part, we give detailed descriptions about the strategy to experimentally retrieve the transmission efficiency of our nanophotonic beam splitter and the on-chip polarized used in our experiment. As stated in the manuscript, the on-chip polarizer gives us a knowledge of the polarization state of light launched in the input waveguide.

4.1 Efficiency calculation in measurement

In order to derive the transmission efficiency of the metamaterial polarization beam splitter (PBS), some reference structures are employed. The measured transmission efficiency is calculated as:

$$\eta_{tot} = \eta_{butt} \cdot \eta_{tapper} \cdot \eta_{PBS}. \quad (1)$$

Here, η_{tot} is the measured fiber-to-fiber coupling efficiency, η_{butt} is the butt-coupling efficiency of fiber to waveguide, and η_{tapper} is the transmission efficiency for the 4μm-long tapper. η_{PBS} is the transmission efficiency of PBS. A straight waveguide without any patterns is employed to measure the butt-coupling efficiency. A straight waveguide with a pair of tappers is used to measure the transmission efficiency of tapper. As a result, the absolute transmission efficiency for PBS is derived by normalizing the total measured transmission efficiency with the measured butting coupling efficiency and transmission efficiency for the tapper.

4.2 On-chip polarizer

As mentioned in the manuscript, we have used an on-chip polarizer to control the polarization state of light launched in the input waveguide. The on-chip polarizer employed here is a pretty straightforward one that is consist of a straight waveguide with a vertical air slot near the center of the waveguide. The center of the air slot exhibits a 70nm offset with regard to the center of the waveguide. The structure as well as the field pattern for the on-chip polarizer are summarized on Fig. S10. For the on-chip polarizer employed in our experiment, TM is transmitted efficiently while TE is blocked as shown in Figs. 10 (c)-(d).

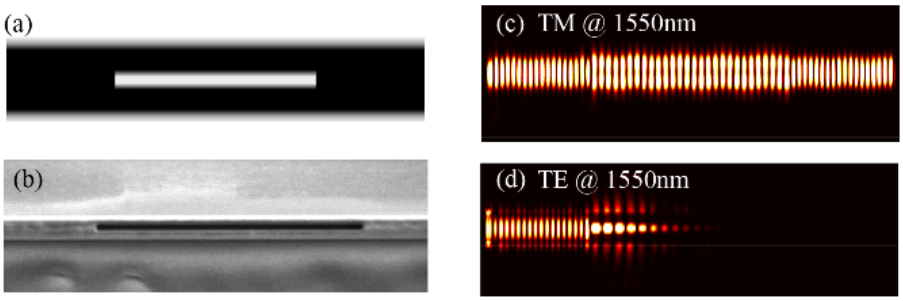

Fig. S10. On-chip polarizer. (a) Epsilon distribution of the design. (b) Scanning-electron micrograph of fabricated on-chip polarizer. (c)-(d) Field patterns for TM and TE, respectively.

5. Movie description

Two movies are provided as supplementary information. Media 1 shows the simulated time evolution of the electric field pattern within the experimental metamaterial polarization beam splitter for TM and TE polarization state, respectively. While Media 2 shows the simulated time evolution of the electric field pattern within the mode converting PBS for both polarization states. In both the two movies, the axis shows the dimension of the structure and is in the unit of micrometer. The White lines, on the other hand, shows the contour plot of the permittivity distribution of the design. Light propagates from left to right.

6. Fabrication Steps

First, we used the Heidelberg MicroPG 101 (laser pattern generator) to pattern 3μm-wide waveguides in positive photoresist (Shipley 1813). The exposure power was 10mW at 65% duration factor and the bi-directional mode was employed. Standard 352B developer was

DOI: 10.1038/NPHOTON.2015.80

used to develop the photoresist for 1min. Then, an Oxford 100 reactive-ion etcher (RIE) was used to etch the silicon. The gas was a mixture of SF_6 with a flow rate of 40ccm and C_4F_8 with a flow rate of 17.5ccm. SF_6 is used for etching the silicon, while C_4F_8 is used for passivation during etching in order to attain straight sidewalls. For our sample, the total etch time was 164 seconds that corresponds to an etch rate of 1.83nm per second. Then, we used the dual-beam focused-ion-beam (FIB, FEI, Helios 650) system to define the nanophotonic PBS, the input/output waveguide and any associated tapers. The nanophotonic PBS has a minimum feature size of 120nm, which can be readily achieved with the FIB tool. The ion beam accelerating voltage was 30kV for all devices. For the nanophotonic PBS, the beam current used was 7.7pA with fluence of $800C/m^2$. Alignment marks fabricated at the same time as the 3μm-wide waveguides were used to ensure that the nanophotonic PBS was aligned with the waveguides.

References

1. G. Kim, J.-A. Dominguez-Caballero, H. Lee, D. J. Friedman, and R. Menon, “Increased photovoltaic power output via diffractive spectrum separation,” Phys. Rev. Lett. 110(12), 123901 (2013).
2. B. Shen, P. Wang, R. Polson, and R. Menon, "Integrated metamaterials for efficient and compact free-space-to-waveguide coupling," Opt. Express 22(22), 27175-27182 (2014).
3. B. Shen, P. Wang, R. Polson, and R. Menon, "Ultra-high-efficiency metamaterial polarizer," Optica 1(5), 356-360 (2014).
4. J. Lu and J. Vučković, “Nanophotonic computational design,” Opt. Express 21(11), 13351–13367 (2013).
5. M. A. Seldowitz, J. P. Allebach, and D. W. Sweeney, “Synthesis of digital holograms by direct binary search,” Appl. Opt.26(14), 2788–2798 (1987).